https://doi.org/10.15407/ufm.20.04.672

I.M. PAZUKHA, V.V. SHCHOTKIN, and Yu.O. SHKURDODA
Sumy State University,
2, Rymskyi-Korsakov Str., UA-40007 Sumy, Ukraine

STRUCTURE, MAGNETIC AND MAGNETORESISTIVE PROPERTIES OF COMPOSITE MATERIALS BASED ON FERROMAGNETIC METALS AND ALLOYS WITH DIFFERENT TYPES OF DIELECTRIC MATRIX

A literary review of the experimental results concerning phase state and crystal structure, magnetoresistive and magnetic properties of the thin-film composite materials formed on the base of granules of ferromagnetic Co metal or Fe_xCo_{1-x} alloy embedded into the insulator matrix (SiO, SiO_2, Al_2O_3) *via* different discovery methods is presented. As shown, the value of magnetoresistance, character of its field dependences and magnetic characteristics depend on the concentration and size distribution of ferromagnetic granules. At the specified conditions, the perpendicular anisotropy can be realized in the structures as ferromagnetic granule–insulator matrix; the reasons of such anisotropy are analysed.

Keywords: composite, ferromagnetic material, insulator matrix, magnetoresistance, magnetic properties.

1. Introduction

The fundamental research of the physical properties of new nanosize functional materials (granular film alloys [2, 3], composites [4], arrays of magnetic nanoparticles [5], vacuum tunnel structures [6]), as well as graphene material that can become an effective substitute for metallic conductive matrices [7], is still actual in the context of the development of the elemental base of spintronics [1]. As it was shown by the analysis of previous studies [8–11], the combination of materials of the ferromagnetic component and conducting matrix makes possible to form structures

that combine high saturation fields with high thermostability, allows realizing the effect of high magnetotransmission. Generally, Refs. [8–11] aimed at studying the phase state, crystal structure, magnetoresistive properties of composite materials based on ferromagnetic materials with different types of a non-magnetic matrix (metallic or insulator). It was shown (see, *e.g.*, Ref. [8]) that the value of magnetoresistance (MR), coercive force, and saturation field depend significantly on the size of magnetic nanoparticles, their concentration, and distribution in the non-magnetic matrix. A specific feature of the ferromagnetic metal-dielectric composite materials is the realization of the tunnel spin-polarized conductivity that causes the appearance of the tunnel magnetoresistance [12]. At the same time, the probability of occurrence of this effect and its magnitude essentially depends on the components volume fraction that is part of their composition. An important question becomes the percolation threshold, in the transition through which there is a change like composite material conductivity. This is due to the difference in the conductivity mechanisms of the metal (the processes of scattering in the volume of metal granules) and insulator (tunnelling between the granules through insulator channels) phases, its magnetic and magnetoresistive properties.

It is importantly from the point of view both problems of the physics of magnetism and the applied aspect are the study of superparamagnetic $\rightarrow$ superferromagnetic $\rightarrow$ ferromagnetic transformations for the magnetic component [13]. As known [14], all magnetic nanoparticles, depending on the critical sizes $D_1(T)$ and $D_2(T)$, can be divided into three categories: superparamagnetic, single-domain, and multi-domain ferromagnetic. Here, $D_1(T)$ is a critical size between superparamagnetic granules and single-domain particles at a certain temperature called blocking temperature, while $D_2(T)$ is a critical size between single-domain ferromagnetic granules and multi-domain particles. All three above-mentioned species of nanoparticles have different magnetic properties under the applied field and affect differently on the magnetoresistive effects.

For instance, the Co nanoparticles with sizes that do not exceed a certain critical value, exhibit superparamagnetism due to their low energy of magnetic anisotropy in single domains. Within the limits of single-domain particles, magnetic moments change the direction in the case when their thermal energy is greater than the energy of magnetic anisotropy. Thus, the behaviour in a magnetic field of an ensemble of this kind of single-domain particles has a paramagnetic nature. It is well known [15] that paramagnetic nanoparticles are not suitable for memory storage since thermal fluctuations lead to the loss of stored data. To stabilize the residual magnetization at a zero external magnetic field, the Si nanoparticles are introduced into the antiferromagnetic matrix, *e.g.*, a SiO_2 matrix [15].

Significant interest in Fe_xCo_{1-x} film alloys arose after the discovery of the giant magnetoresistance effect in multilayer systems based on ferromagnetic layers with nonmagnetic interlayers. They have widely used as elements of various types of equipment and devices of modern electronics [16]. In this case, the research of magnetoresistive and magnetic properties of composite materials based on Fe_xCo_{1-x} introduced into the insulator matrix as a magnetic material with high resistivity, saturation magnetization, permeability in the high-frequency range, and a high frequency of ferromagnetic resonance [17] remain relevant.

The goal of this work is to summarize the data on the phase state, crystal structure, magnetic and magnetoresistive properties of composite materials formed on the basis of the ferromagnetic materials' granules (Co, Fe_xCo_{1-x}) and insulator matrix (SiO, SiO_2, Al_2O_3) by using different methods depending on the thickness of samples, their composition and heat treatment conditions (regime).

2. Structure of the Ferromagnetic–Insulator-Type Composite Materials

Typically, for the formation of composite materials of a ferromagnetic–insulator-type, different methods are used. These methods allow realization of simultaneous deposition on the substrate of the metal and insulator components (magnetron, ion-beam, resistive, *etc*.) [18], as well as such as sol–gel and ion implantation methods [19, 20].

Cross-section TEM images of thin film sample with a total thickness of 30 nm prepared by the co-evaporation technique of Co and SiO at x_{Co} = 83.33% [21] presented in Fig. 1, *a*. The sample consists of Co nanogranules, between which channels with SiO are formed. According to Ref. [21], the reason for the segregation of SiO on the Co granules surface is to decrease the system energy, since the surface energy of SiO is much lower than Co. The average size of magnetic component grains, which evenly distributed in the matrix of the insulator material, is circa 6 nm.

The method for the formation of composite materials by condensation of a multilayer structure $Co(0.7)/SiO_2(3)]_{10}/SiO_2(10)/Si$ (the thickness in the brackets is in nm) with ultra-thin layers is proposed in Ref. [22]. An additional buffer layer of SiO_2 with a thickness of 10 nm application leads to three-dimensional growth of the Co granules in the form of spherical clusters. According to Ref. [22], such growth of the magnetic material on the buffer layer surface is due to the difference between the surface energies of Co and SiO_2. The next layer of amorphous SiO_2 perfectly wets this granular Co layer, resulting in a surface layer having a wave shape. At the next Co layer condensation, the formation of clusters occurs predominantly on the grooves of the surface roughness. The periodic repetition of the condensation of Co and amorphous SiO_2

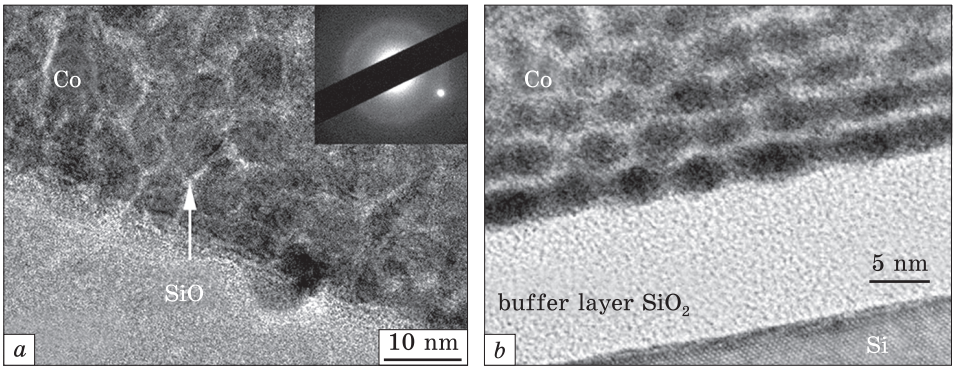

Fig. 1. Cross-section TEM images of thin film sample with the total thickness of 30 nm prepared by the co-evaporation technique of Co and SiO at $x_{Co} = 83.33\%$ [21] (*a*), and $[Co(0.7)/SiO_2(3)]_{10}/SiO_2/Si$ multilayer thin film structure [22] (*b*) after condensation

layers results in the multilayer structure with self-organizing growth (Fig. 1, *b*) [22]. The average size of the Co grains for the $Co(0.7)/SiO_2(3)]_{10}/SiO_2(10)/Si$ structure does not exceed 3 nm.

Important for further analysis of the magnetic properties of composite materials is the phase state of the magnetic components. As well known, for Co, a low-temperature h.c.p. phase is stabilized in a bulk state. The polymorphic transition from h.c.p. Co to f.c.c. Co occurs at the temperatures of 690–700 K. However, the different phase state can stabilize in Co granules depending on their size in the as-deposited state [23–26]. The h.c.p. phase is stabilized only for granules with the size of more than 40 nm. Simultaneously h.c.p. and f.c.c. phases have observed if the granule size varies in the range from 20 to 40 nm. Besides, for granules with an average size of less than 20 nm, there is an f.c.c.-phase only. It should also be taken into account that the embedding of Co into the insulator matrix can change the ranges of granular sizes in which the f.c.c. and h.c.p. phases are stabilized [27–29].

The results of the phase state and crystal structure investigations [30] of as-deposited and annealed at a temperature of 700 K Fe_xCo_{1-x} thin film alloy is given in Fig. 2. According to the data of electron microscopic and electrographic studies, for as-deposited (Fig. 2, *a*, *b*) and annealed at a temperature of 700 K (Fig. 2, *d*, *e*) single-layer samples with the thickness $d = 10–80$ and $x > 30$ at.%, the phase state corresponds to the b.c.c. Fe_xCo_{1-x} with a lattice parameter $a = 0.292–0.293$ nm. At the electron diffraction patterns, for as-deposited films with $x < 30$ at.%, the lines that correspond to the reflection from the crystallographic planes of the b.c.c. and h.c.p. lattices are fixed (Fig. 2, *c*). The phase state of such samples corresponds to the combination of solid solution (s.s.) b.c.c.-Fe_xCo_{1-x} + h.c.p.-Co with a lattice parameters $a_{s.s.} = 0.291–0.294$ nm

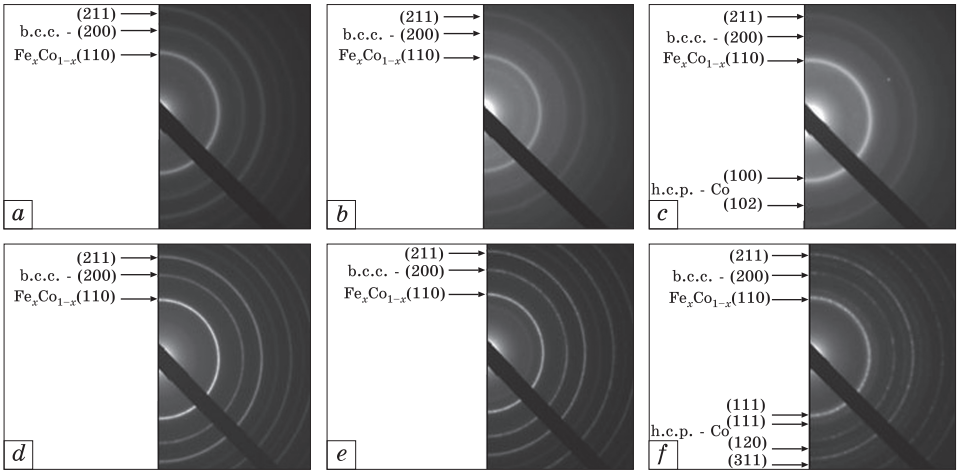

Fig. 2. Electron diffraction patterns of Fe_xCo_{1-x} single-layer thin films (d = 50 nm) at as-deposited (a–c) and annealed at the temperature of 700 K (d–f) states, where $x \cong 80$ (a, d), $x \cong 50$ (b, e), and $x \cong 20$ at.% (c, f) [30]

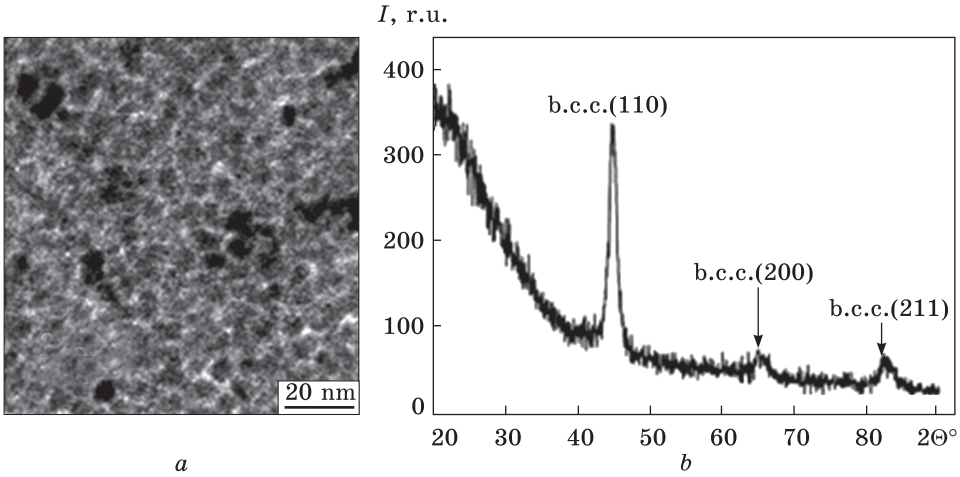

Fig. 3. TEM image (*a*) and XRD spectrum (*b*) for thin film sample based on ferromagnetic alloy $Fe_{65}Co_{35}$ and insulator matrix SiO_2. The concentration of the magnetic component in the sample is x = 60 vol.%; the total thickness is 300 nm [17]

and a_{Co} = 0.250–0.253 nm, c = 0.410–0.413 nm, respectively. The analysis of diffraction images for thin film alloys after the heat treatment up to a temperature of 700 K indicates the presence of lines belonging to the f.c.c.-phase. Hence, thin-film alloys after the heat treatment also have a two-phase state b.c.c.-Fe_xCo_{1-x} + f.c.c.-Co. Regarding the fixation of f.c.c. Co below the temperature of the polymorphic transition in the Co bulk state (T = 690–700 K), the authors [30] outline two possible

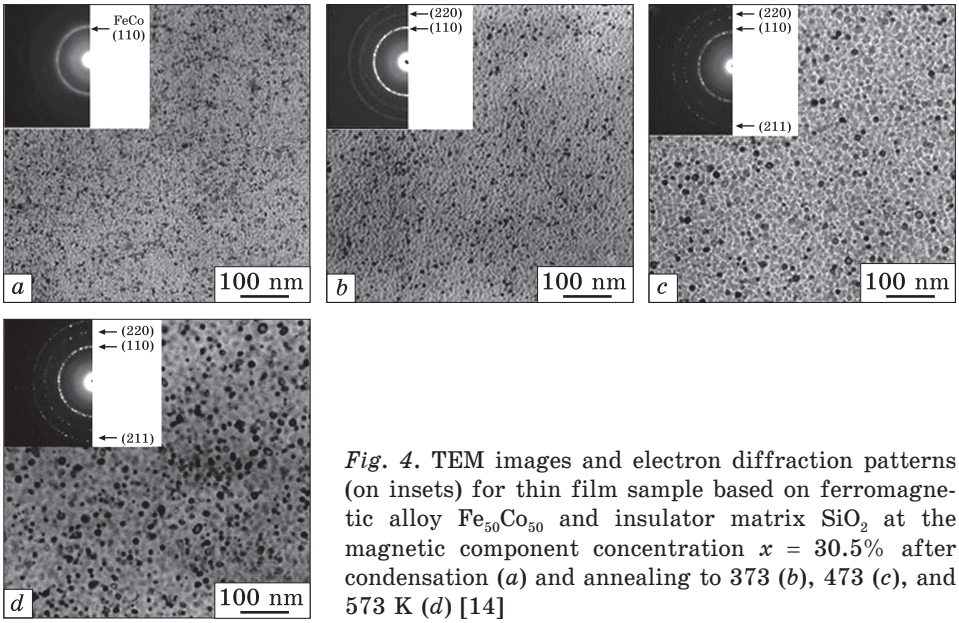

Fig. 4. TEM images and electron diffraction patterns (on insets) for thin film sample based on ferromagnetic alloy $Fe_{50}Co_{50}$ and insulator matrix SiO_2 at the magnetic component concentration x = 30.5% after condensation (*a*) and annealing to 373 (*b*), 473 (*c*), and 573 K (*d*) [14]

reasons. The first one is the high-temperature phase of stabilizes either as a metastable. The second one is reflections from the f.c.c.-Co correspond to the scattering from the set of packaging defects in h.c.p. Co, which has an f.c.c. structure.

Figure 3 illustrates the transmission electron microscopy (TEM) image and x-ray diffraction (XRD) spectrum for thin-film sample based on ferromagnetic alloy $Fe_{65}Co_{35}$ and insulator matrix SiO_2 with a total thickness of 300 nm (the concentration of the magnetic component in the sample is x = 60 vol.%) [16]. The X-ray pattern fixes the b.c.c. phase that corresponds to the $Fe_{65}Co_{35}$ alloy, and the insulator component is in an amorphous state. The average size of the magnetic component grains is 6.2 nm, and the width of the dielectric channels is 1 nm. For a system based on ferromagnetic alloy $Fe_{65}Co_{35}$ and insulator matrix SiO_2 at $x_{Fe_{65}Co_{35}}$ = 30.5 vol.%, only the b.c.c. phase that corresponds to the FeCo granules with the average size of 3.3 nm fixed at the diffraction images [13]. The heat treatment process up to 573 K leads to a monotonous increase of their size by 1.5 times (Fig. 4).

3. Magnetoresistive Properties

A perspective direction in the development of the physics of devices, elements, and systems is the investigation of metal–insulator tunnel structures, due to the wide possibilities of their practical use. A characteristic feature of magnetoresistive properties composite materials such as ferromagnetic–insulator is the presence of a tunnel spin-depen-

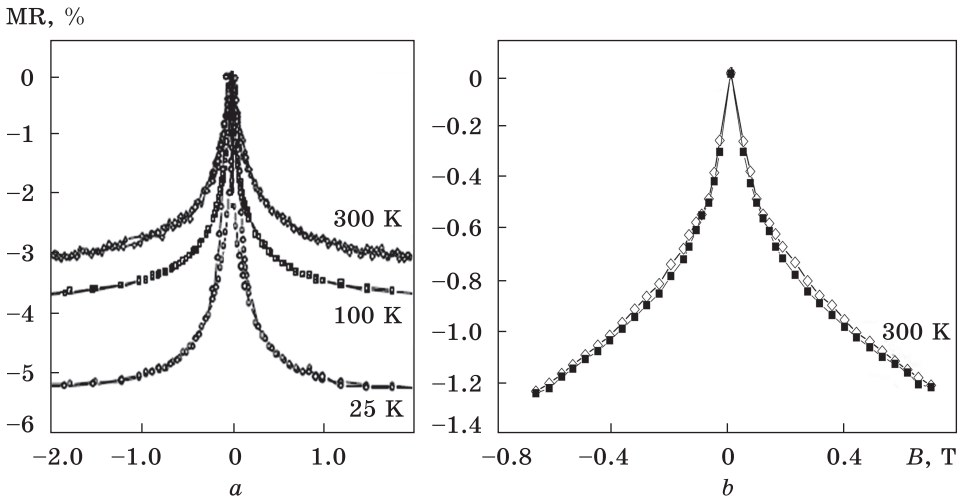

Fig. 5. Field dependences of magnetoresistance for $[Co(0.7)SiO_2(3)]_{10}/SiO_2/Si$ multilayer thin film systems (the measurement temperature is 25, 100, and 300 K) [22] (*a*) and for Co- and SiO_2-based composite prepared by the co-evaporation technique (c_{Co} = 50 at.%, d = 30 nm, the measurement temperature is 300 K) [34] (*b*)

dent conductivity, which leads to the appearance of the tunnelling magnetoresistance effect (TMR) [31]. Such structures include composites based on Co nanoparticles or alloys Fe_xCo_{1-x} in insulator matrices SiO_2, SiO, or Al_2O_3. The TMR effect in such systems reaches several percents at a room temperature under magnetic fields up to 1 T [21, 32, 33].

Figure 5 shows field dependences of magnetoresistance (MR) for composite materials prepared by the methods of layered condensation (the initial structure is $[Co(0.7)SiO_2(3)]_{10}/SiO_2/Si$ [22]) and co-evaporation techniques (c_{Co} = 50 at.%, d = 30 nm) [34].

From the shown graphs of the MR(B), which were carried out at temperatures of 25, 100 and 300 K, it follows that the magnetoresistance is isotropic for both layered and simultaneous condensation.

In this case, composite materials that consist of ferromagnetic nanoparticles embedded in the insulator matrix can be considered as a system that contains a large number of nanosize tunnel junctions [31]. The value of the tunnelling conductivity depends on the distribution of the metal particles size and the width of the insulator channels. Therefore, the magnetoresistance value due to electrons spin-dependent tunnelling through the insulator channels will depend on the magnetic particles size and their distribution in the volume of the dielectric matrix. It should be stressed that depending on the state (superparamagnetic, single-domain, or multi-domain ferromagnetic), magnetic nanoparticles can show different magnetic properties at an applied magnetic field and affect differently the processes of spin-dependent scattering.

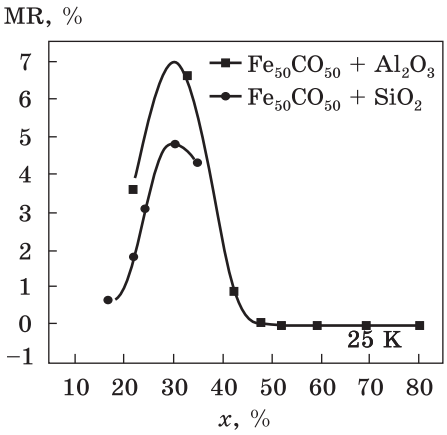

Fig. 6. Concentration-dependent magnetoresistance for $(Fe_{50}Co_{50}+Al_2O_3)/S$ and $(Fe_{50}Co_{50} + SiO_2)/S$ thin film composite [37]

Theoretical and experimental investigations of the giant magnetoresistive effect in metal composites have shown [35–38] that the presence of multi-domain ferromagnetic nanoparticles play a negative role in its realization, while superparamagnetic nanoparticles play a key role [35]. In this case, the authors of Ref. [36] found that there is no definite monotonic relationship between the sizes of nanoparticles and the magnitude of the effect. For each specific system, in which the GMR realized, the maximum value of the effect is fixed at a certain average magnetic nanoparticles size for the given temperature of the heat treatment. This indicates that single-domain nanoparticles, rather than superparamagnetic, predominate in the magnetoresistive effect realization. Since the TMR originates from spin-dependent tunnelling between magnetic metal nanoparticles or granules through insulating channels in the case when the magnetic component concentration is lower than the percolation threshold, therefore their size and magnetic state metal of nanoparticles have to be taken into account as well. Thus, the authors of Ref. [37] proposed a phenomenological theoretical model describing a giant tunnelling MR in nanosize metal–insulator structures. This model takes into account the influence of insulator matrix type on the processes of spin polarization of ferromagnetic nanoparticles and, as a result, on the tunnelling magnetoresistive effect. In addition, in Ref. [37], an effort to take into account the contribution of single-domain nanoparticles concerning superparamagnetic in the tunnel magnetoresistance magnitude of the metal–insulator composites was attempted. The comparative analysis [38] of the calculation and experimental data for the $Fe + Al_2O_3$ and $Fe_{50}Co_{50} + SiO_2$ systems showed that a satisfactory agreement of the proposed model with the experiment is observed only if single-domain ferromagnetic nanoparticles play a key role in the TMR effect realization.

The influence of the concentration of component on the magnetoresistive properties of composite materials considered in this paper is also associated with the change of the average size of magnetic granules as the composition of the system changes. As seen in Fig. 6, the dependence of MR(x) is characterized by the presence of a clearly expressed maximum [41] for both the film metal composites [39] and granular

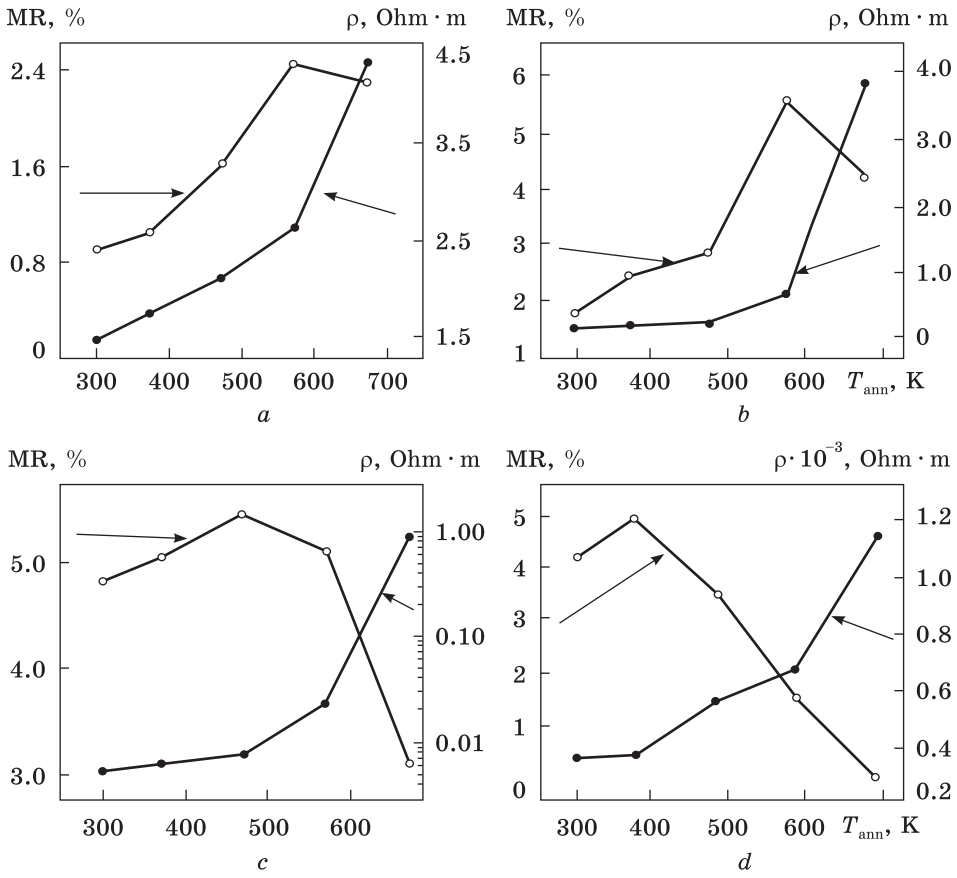

Fig. 7. The dependence of magnetoresistance and the resistivity in the absence of applied fields on the annealing temperature for $Fe_{50}Co_{50}$- and SiO_2-based thin film composite at the magnetic material concentration x = 17 (*a*), 24 (*b*), 30 (*c*), and 39 vol.% (*d*) [14]

alloys [40]. This factor indicates that the necessary conditions for the charge carriers tunnelling were realized. Figure 7 shows the heat treatment effect (up to 700 K) on the magnetoresistance and resistivity value for composite based on $Fe_{50}Co_{50}$ and SiO_2 at different concentrations of magnetic material [13]. As shown, with increasing of annealing temperature, MR for samples with less content of $Fe_{50}Co_{50}$, reaches a maximum at the higher annealing temperature. According to Refs. [37, 38], such behaviour of the magnetoresistance can be explained by the fact that single-domain ferromagnetic granules play a key role in the magnetoresistive effect value.

The interest in the ferromagnetic–insulator composites is also conditioned by the possibility of realization in them of both negative and positive isotropic magnetoresistance [42, 43] in the narrow region of

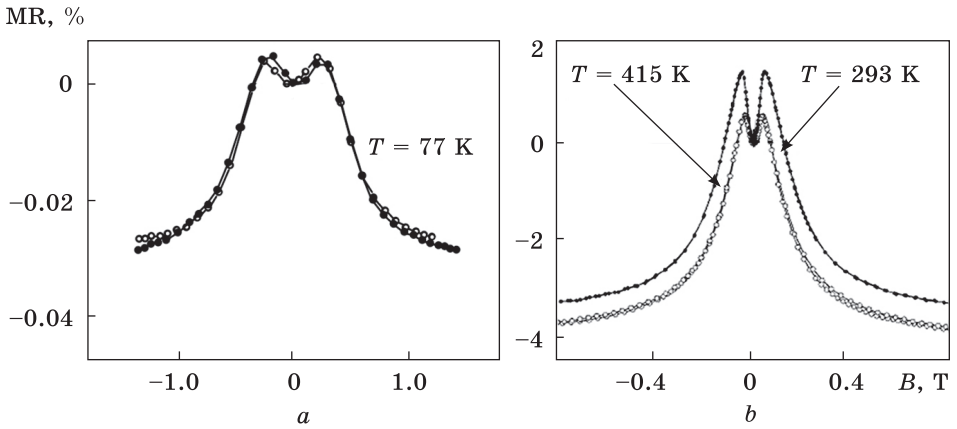

Fig. 8. Field-dependent magnetoresistance for Co- and SiO_2-based composite at x_{Co} = 43% (*a*) [41] along with Co- and Al_2O_n-based composite at x_{Co} = 58% (*b*) [42]

concentrations near the percolation threshold. As can be seen in Fig. 8, two maximums in the magnetic field up to 0.1 T are observed on the magnetic field dependences. At the same time, these given maximums are observed with a decrease in the measurement temperature of 77 K and after heat treatment of the samples. The possible reason for these maximum appearing is the fact that the structure of thin-film composite materials near the percolation threshold is characterized by the presence of both isolated nanogranules and ferromagnetic clusters formed due to their coalescence. Granules and clusters are characterized by different values of the energy of magnetic anisotropy. Besides, a strong dipole–dipole interaction exists between them. Because of the increase of the local magnetic moments, the disordering under the weak magnetic fields occurs which leads to the maximum appearance.

The diagrams of the tunnelling current flow for different values of the induction of an external magnetic field under strong, zero, and weak magnetic fields are presented in Fig. 9. It allows understanding the mechanism of a positive isotropic MR appearance in the ferromagnetic–insulator composite.

In the case of a strong field, the magnetic moments of the magnetic granules and clusters are oriented in a parallel geometry to each other (cluster *A* and granules *B*, *D* in Fig. 9, *a*). In the case, when the magnetic moments of the granules are oriented in one direction, the probability of electrons tunnelling between two adjacent magnetic granules will maximize. Therefore, this creates favourable conditions for the charge carriers tunnelling [44]. The electrical resistance of such a system will be minimal.

In the case of a zero field, the magnetic moments of isolated granules direct along the axes of easy magnetization. At the same time, if the

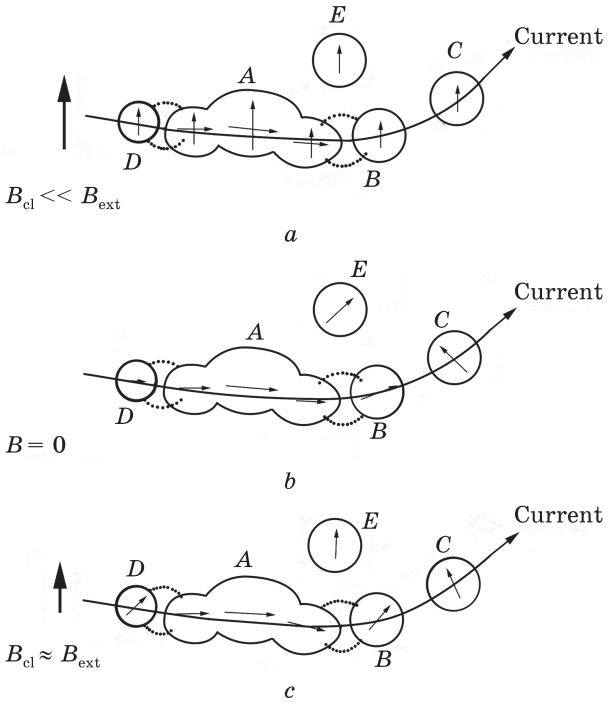

Fig. 9. The diagrams of tunnelling current flow for different values of the induction of an external magnetic field under strong (*a*), zero (*b*), and weak (*c*) magnetic fields, where B_{ext} is the external magnetic field, B_{cl} is the field created by the magnetic moment of the cluster [40]

concentration of the magnetic component is insignificant (much lower than the percolation threshold), the axes of easy magnetization of composite material granules randomly direct relative to each other. Consequently, in the zero fields, the magnetic moments of granules maximally disordered. It leads to an increase of resistance. Increasing of the concentration of the magnetic component to a value close to the percolation threshold causes the decrease of the width of the dielectric channels, the association of the granules, and the formation of magnetic clusters. This leads to the appearance of dipole–dipole interaction that affects the orientation of magnetic moments of granules and clusters. Due to the occurrence of anisotropic form, the magnetic moment of the cluster will direct along its long axis. Since the energy of magnetic anisotropy for a cluster is greater than the energy of anisotropy for a single granule, the dipole–dipole interaction will influence on the orientation of magnetic moments of the granules located near the cluster.

Thus, the regions of the same orientation of the magnetic moments of the magnetic clusters and adjacent granules (cluster *A* and granule *B* in Fig. 9, *b*) are formed in the sample. In contrast to the composite with a magnetic component concentration far from the percolation threshold, the resistance of such a sample will not reach the maximum value in a zero field. At the remagnetization of the samples in case of a weak magnetic field, the magnetic moments of the granules, located at a

certain distance from the cluster (*B*), begin to orient along the field. At the same time, the magnetic moment's orientation of the granule (*D*, *B*) located near the cluster is determined by the minimum of internal energy and non-collinear direction of the cluster magnetic moment or the external magnetic field direction (Fig. 9, *c*). Hence, the maximum degree of the disordering of magnetic moments is realized in the weak fields (close to the fields created by clusters in the nearest surround). As a result, the system is characterized by the greatest resistance value.

4. Magnetic Properties

A considerable amount of works have been devoted to the study of the magnetic properties of composite film materials based on ferromagnetic Co or Co_xFe_{1-x} materials embedded in different types of insulator matrices (SiO, SiO_2, Al_2O_3) (see Refs. [41, 45–51]). Note that Fe–Co is applied in the engineering as a soft magnetic material with both magnetic components, comparably large value of the magnetic saturation and Curie temperature (see [52, 53] and Refs. therein). As a rule, a detailed information about the magnetic state of films is obtained from magnetic measurements using SQUID (temperature range 5–300 K) or vibrating magnetometers (temperature range 90–300 K) in a magnetic field up to 1 T [46, 50].

For example, concentration and the heat treatment effects on the magnetic properties of $(Fe_{50}Co_{50}+SiO_2)/S$ (*S* is a substrate) composites were analysed in Refs. [14, 17]. It is shown, that the magnitude of the coercive force B_c does not exceed 1.8 mT in the concentration range of the magnetic component $x = 52–80\%$ and reaches its minimum value of 0.78 mT at $x = 60\%$ (Fig. 10, *a*). The process of thermal annealing leads

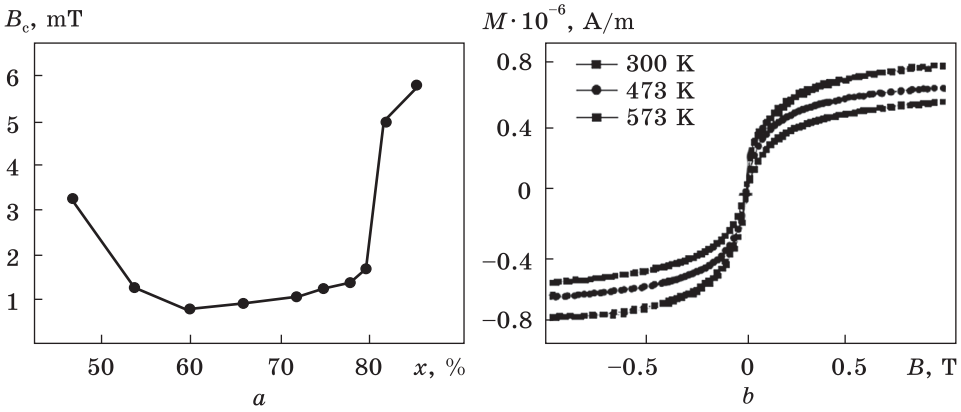

Fig. 10. The coercivity (B_c) *vs*. the concentration of magnetic component (x) for $(Fe_{50}Co_{50}+SiO_2)/S$ composite [17] (*a*), and the magnetization curves for $(Fe_{50}Co_{50}+SiO_2)/S$ composite at $x = 30.5$ vol.% after condensation and heat treatment to 473 and 573 K [14] (*b*)

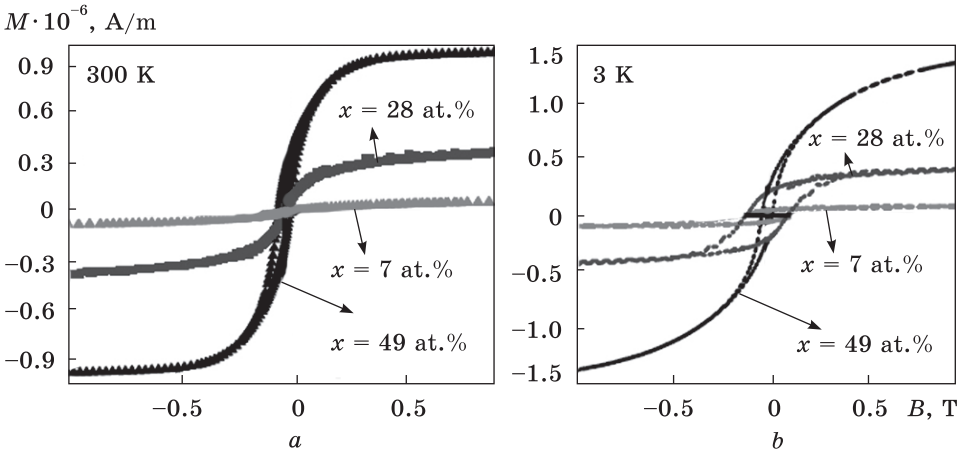

Fig. 11. The dependence of magnetization on the external magnetic field strength at the longitudinal measurement geometry along the direction of magnetization easy axis for Co- and SiO_2-based composite material measured at 300 K (*a*) and 3 K (*b*) for concentrations x_{Co} = 7 at.%, 28 at.%, and 49 at.% [15]

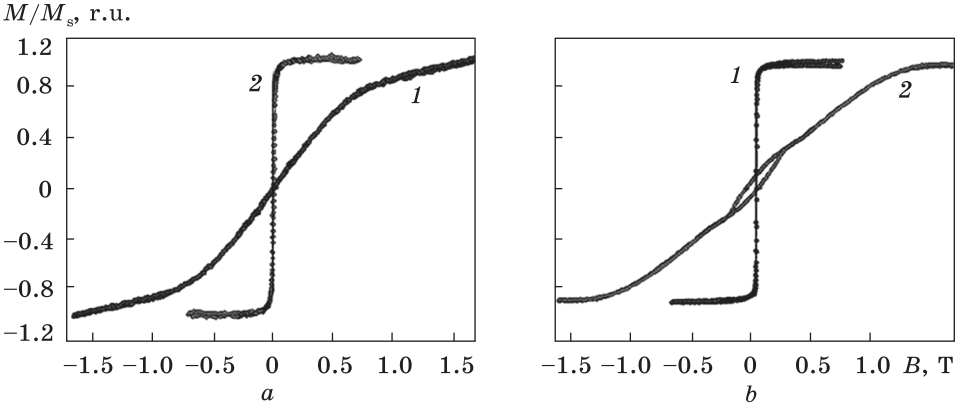

Fig. 12. Normalized magnetization as a function of the applied field at the 'in-plane' (*1*) and 'out-of-plane' (*2*) applied magnetic fields for Co- and SiO-based composites with the total thickness of 30 nm at x_{Co} = 50 at.% (*a*) and 90 at.% (*b*) [34]

to an increase in both the saturation magnetization and the magnetic susceptibility (Fig. 10, *b*).

Results of the study of the magnetic properties of composite film materials based on Co and SiO_2 are presented in Figs. 11 and 12 [15, 34]. The analysis of magnetization curves showed that their shape and the magnetic parameters (residual magnetization, saturation magnetization, coercive force, and saturation field) also depend on the Co concentration (x_{Co}) and the measurement temperature.

It should also be noted that the analysis of the results of magnetostatic studies of granular films made at room temperature for magnetization

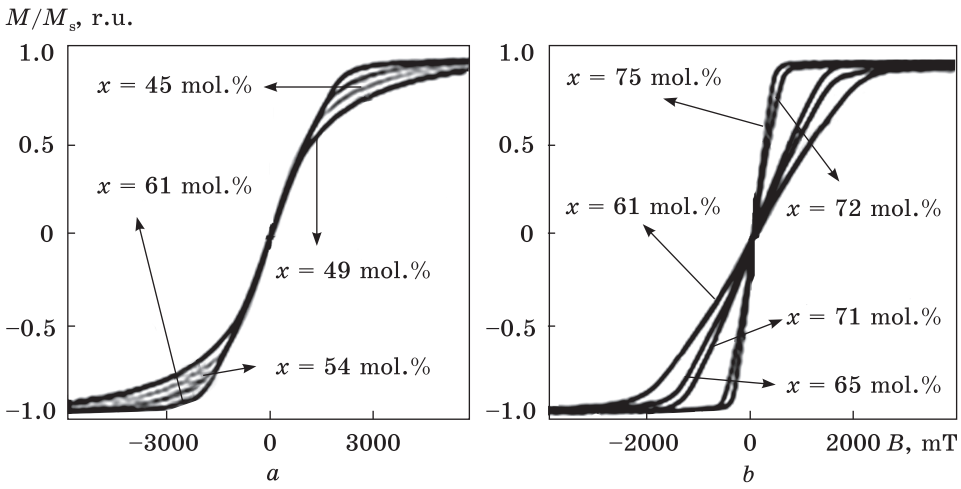

Fig. 13. The magnetization curves for 'in-plane' magnetization at T = 300 K for Co- and Al_2O_3-based sample with different concentration of magnetic component (x) [45]

in the plane of the film showed that by the concentration of ferromagnetic metal or alloy in the films, all the samples can be divided into three groups [46]

Much lower of the percolation threshold ($x < 40$ mol.%), the magnetization curves are typical for the superparamagnetic state. The shape and slope of the curve near the zero magnetic fields are modified depending on the ferromagnetic material concentration and the measurement temperature. Within the concentration range of $44 < x < 61$ mol.%, the magnetization curves (Fig. 13, *a*) have a characteristic slope in small fields almost independently on the Co concentration and temperature. It is noteworthy that the dependence of the magnetization on the magnetic field in a quite wide range of fields is linear. The range of fields, in which it retains its linearity, increases due to the increase of the Co concentration and reaching its maximum value for samples with a cobalt concentration of 61 mol.% (Fig. 13). This behaviour may be attributed to the presence of uniaxial anisotropy of the granules, crystallographically or anisotropically related to the shape of the particles in the film having the predominant orientation of their easy axes magnetization in a direction perpendicular to the film plane. Additional experimental study of these samples showed that the curves' shape is not changed at the 'in-plane' magnetization at different directions of the magnetic field in the film plane. Thus, it should be assumed that a uniaxial anisotropy with easy axis magnetization oriented perpendicular to the film plane is formed in these samples during the condensation processes. It should also be noted that the perpendicular anisotropy field for the sample with a concentration of Co x = 61 mol.% with extrapolation of the linear

section of magnetization exceeds 200 mT. For higher concentrations ($x > 61$ mol.%), the magnetization curves (Fig. 13, *b*) retain linearity and all characteristic features of 'hard' magnetization, but the effective field of perpendicular anisotropy with increasing Co concentration will be decreased. Considering that, in this concentration range, the transition of a granular system through the percolation threshold occurs; the change in the value of perpendicular anisotropy is associated with an increase of intergranular interaction, which forms a collective state, whose magnetic properties begin to dominate over the properties of individual granules.

It should be noted that the occurrence of perpendicular anisotropy in granular films with a thickness much larger than the size of the granules is a rare phenomenon, which is described only in several works [41, 46, 51]. Self-organization of the granular state during the film growth is a rather complicated process, which depends on many technological parameters. Therefore, an unambiguous interpretation of the nature of this perpendicular anisotropy requires not only magnetic studies but also analysis of phase and crystal state, electron microscopy, magnetic force microscopy data, *etc*. However, the most probable reasons for the nature of anisotropy may be two of them.

The first one is the formation of elongated, 'columnar' form of granules in the process of growth. Then the anisotropy of the granule shape, with the easy axis of magnetization is oriented perpendicular to the film plane, will determine the magnetic anisotropy magnitude. During the growth process, for compositions lower the percolation threshold, the formation of granular structures was observed. This structure consists of amorphous granules or granules with a cubic crystalline structure whose crystallographic anisotropy is small for Co. These granules are in the form of uniaxial ellipsoids with elongated axes oriented perpendicularly to the film plane. Their form remains unchanged as the concentration increases. Above the percolation threshold, the granules begin to coalesce, which reduces the anisotropy of their resulting form and, respectively, the magnetic anisotropy. In this case, the question of the weak dependence of the anisotropy of the granule shape on the concentration lower the percolation threshold remains unclear. The rather high value of the percolation threshold in these systems is evidence to the precisely oriented anisotropy of the granule shape.

The second possible reason is the crystallographic anisotropy inside the granules. If Co granules have a hexagonal phase with high crystallographic anisotropy, then such granules can have considerable variation in shape and size, but crystallographic anisotropy will be the same for all. It will be oriented if all the granules grow in a hexagonal phase with equally directed axes of easy magnetization. In the cases considered above, this direction is perpendicular to the plane of the film, which is

a low-probable event. Cooling to the room temperature is accompanied with the appearance of some deformation perpendicular to the film plane. It is due to the different coefficients of thermal expansion of the film and the substrate. This could be the cause of the granular structural transformation from the amorphous phase to hexagonal one with the direction of its orientation along the strain direction. However, assuming the crystallographic nature of the anisotropy of granules, the quite low value of perpendicular anisotropy is not quite clear. According to Ref. [46], the anisotropy field of h.c.p. Co is approximately 950 mT. The maximum value of perpendicular anisotropy in the considered films is three times less. It could be assumed that the hexagonal axes of the granules only partially oriented along the normal to the film. In addition to the manifestations of perpendicular anisotropy, the characteristic indications of randomly oriented anisotropy of the granules would have to be observed in the magnetization curves. The electron diffraction investigations show that granules are crystalline, and there is no orientation of their crystallographic axes. Besides, with such an assumption about the origin of the anisotropy normal to the film plane, it is also difficult to explain its decrease at the concentration of the magnetic component above the percolation threshold.

Additional studies for samples with the maximum perpendicular anisotropy value make it clear that perpendicular anisotropy is related to the anisotropy of individual granules rather than the film as a whole. The magnetization curves obtained in the measurement geometries parallel and perpendicular to the film plane show the characteristic behaviour for the multidomain state of the system with magnetization in the domains perpendicular to the plane. In the demagnetized state of the minimum energy of the ensemble with uniaxial single-domain granules with their easy axis magnetization perpendicular to the plane, will correspond to such a magnetic state in which half of the magnetic moments of the granule-domains are oriented parallel to the normal of the film, and the other half is antiparallel to it. That is, the magnitude of the film's magnetization will not be retained when the magnetic field removed. At the sample magnetization by an external field perpendicular to the film, the magnetization increases due to the reorientation of the individual granules moments and the formation of a collective magnetization whose modulus increases linearly with the field.

In addition, the magnetization curves obtained at different temperatures show an increase in coercivity with a decrease in temperature, which is caused by the blocking of the magnetic moments of individual granules. The coercivity of the field reaches the value of 55 mT at $T = 80$ K. For magnetization in perpendicular geometry, the monotonous increase in coercivity for magnetization in perpendicular geometry is accompanied by an increase of coercivity in the parallel geometry of

measurement. Although the coercive field in this case is much smaller and the residual magnetization is very small. The obtained data suggest as follows: (i) the presence of magnetic particles in the ensemble of magnetic nanoparticles; (ii) a slight disorientation of the directions of the axes of easy magnetization of the granules; (iii) the presence of a small part of the granules with another type of anisotropy and/or spatial distribution of their easy magnetization axes.

Another fact that demonstrates the presence of perpendicular anisotropy in the samples is a comparison of the concentration dependence of the magnetization determined by magnetostatic measurements and the magnitude of magnetization found from the measurements of ferromagnetic resonance. In addition to the anisotropy of the granules, the films have an 'easily planar' anisotropy associated with the demagnetization factor of the sample as a whole.

5. Conclusions

The crystal structure and phase state, magnetoresistive, and magnetic properties of Co- and Fe_xCo_{1-x}-based composite films with a different type of insulator matrix (SiO, SiO_2, Al_2O_3) are analysed in this work.

(i) The structure of ferromagnetic metal (Co or Fe_xCo_{1-x})–insulator (SiO, SiO_2, Al_2O_3) composites consists of ferromagnetic granules with an average size of 3–6 nm, separated by insulator channels of 1–2 nm wide. The thermal annealing process results in a monotone increase in the average size of the granules in 1.5 times.

(ii) It is shown that if the content of the magnetic component is $x = 30$–50 at.%, the tunnel magnetoresistive effect is realized in such structures. Amplitude of the effect is defined by the sizes of ferromagnetic granules and insulator channels depending on the component concentrations. The temperature dependences of the magnetoresistance are non-monotonic due to the increase of the size of magnetic granules and width of insulator channels.

(iii) Near the percolation threshold, both negative and positive isotropic magnetoresistance can be realized. The appearance of positive isotropic magnetoresistance in the range of fields up to 0.1 T is due to the peculiarities of the structure of composite materials near the percolation threshold. That is a result of different values of magnetic anisotropy energy in isolated granules and clusters as well as the strong dipole–dipole interaction between them.

(iv) The shape of magnetization curves is determined by the percolation threshold in the system, which, depending on the compositions of the samples, belongs to the range $44 < x < 61$ at.%. This range is characterized by the independent nature of the dependence of $M/M_s(B)$ on the magnetic component concentration and the measurement temperature.

Below this range, the magnetization curves are typical for the superparamagnetic state, and above the range, they preserve linearity and all indications of 'hard' magnetization.

(v) Important for practical application is the appearance of perpendicular anisotropy in this type of composite materials at thicknesses much larger than the size of the granules.

Acknowledgement. The authors acknowledge the Ministry of Education and Science of Ukraine for supporting this work within the framework of the State Budget Program (no. 0119U100777 for 2019–2021).

REFERENCES

1. I.Yu. Protsenko, P.K. Mehta, L.V. Odnodvorets, C.J. Panchal, K.V. Tyschenko, Yu.M. Shabelnyk, and N.I. Shumakova, *J. Nano- Electron. Phys.*, **6**, No. 1: 01031 (2014).
2. Ia.M. Lytvynenko, I.M. Pazukha, and B.B. Bibyk, *J. Nano- Electron. Phys.*, **6**, No. 2: 02014 (2014).
3. A.P. Singh, M. Mishra, and S.K. Dhawan, Conducting multiphase magnetic nanocomposites for microwave shielding application, *Nanomagnetism* (UK: One Central Press: 2014), Ch. 10, p. 246.
4. D. Lisjak and A. Mertelj, *Prog. Mater. Sci.*, **95**: 286 (2018). https://doi.org/10.1016/j.pmatsci.2018.03.003
5. Yu.O. Shkurdoda, I.M. Pazukha, and A.M. Chornous, *Int. J. Min. Metall. Mater.*, **24**, No. 12: 1459 (2017). https://doi.org/10.1007/s12613-017-1539-6
6. L. Vicarelli, S.J. Heerema, C. Dekker, and H.W. Zandbergen, *ACS Nano.*, **9**, No. 4: 3428 (2015). https://doi.org/10.1021/acsnano.5b01762
7. A. Hirohata and K. Takanashi, *J. Phys. D: Appl. Phys.*, **47**, No. 19: 193001 (2014). https://doi.org/10.1088/0022-3727/47/19/193001
8. S.B. Dalavi, J. Theerthagiri, M.M. Raja, and R.N. Panda, *J. Magn. Magn. Mater.*, **344**: 30 (2014). https://doi.org/10.1016/j.jmmm.2013.05.026
9. A.R. Akbashev, A.V. Telegin, A.R. Kaul, and Yu.P. Sukhorukov, *J. Magn. Magn. Mater.*, **384**: 75 (2015). https://doi.org/10.1016/j.jmmm.2015.02.018
10. S. Behrens and I. Appel, *Curr. Opin. Biotechnol.*, **39**: 89 (2016). https://doi.org/10.1016/j.copbio.2016.02.005
11. Yu.I. Dzhezherya, A.F. Kravets, I.M. Kozak, A.Ya. Vovk, and A.M. Pogorily, *J. Nano- Electron. Phys.*, **6**, No. 2: 02027 (2014).
12. X. Li, Y. Li, Y. Shia, F. Du, Y. Bai, Z. Quan, and X. Xu, *Mater. Lett.*, **194**: 227 (2017). https://doi.org/10.1016/j.matlet.2017.02.028
13. D.S. McLachlana, B.T. Doyle, and G. Sauti, *J. Magn. Mater. Magn.*, **458**: 365 (2018). https://doi.org/10.1016/j.jmmm.2018.03.002
14. C. Wang, Y. Zhang, P. Zhang, Y. Rong, and T.Y. Hsu, *J. Magn. Magn. Mater.*, **320**, No. 5: 683 (2008). https://doi.org/10.1016/j.jmmm.2007.08.007

15. R. Walia, J.C. Pivin, A.K. Chawla, R. Jayaganthanc, and R. Chandra, *J. Alloys Compd.*, **509**, No. 6: L103 (2011).
https://doi.org/10.1016/j.jallcom.2010.11.151
16. H. Kockar and M. Alper, *J. Magn. Magn. Mater.*, **373**: 128 (2015).
https://doi.org/10.1016/j.jmmm.2014.03.029
17. D. Yao, S. Ge, and X. Zhou, *Physica B*, **405**, No. 5: 1321 (2010).
https://doi.org/10.1016/j.physb.2009.11.077
18. E. Cattaruzza, G. Battaglin, P. Canton, C. de Julián Fernández, M. Ferroni, F. Gonella, C. Maurizio, P. Riello, C. Sada, C. Sangregorio, and B.F. Scremin, *Appl. Surf. Sci.*, **226**, Nos. 1–3: 62 (2004).
https://doi.org/10.1016/j.apsusc.2003.11.032
19. R. Sen, G. C. Das, and S. Mukherjee, *J. Alloys Compd.*, **490**, Nos. 1–2: 515 (2010).
https://doi.org/10.1016/j.jallcom.2009.10.072
20. P. Gangopadhyay, T. R. Ravindran, B. Sundaravel, K.G.M. Nair, and B.K. Panigrahi, *Nucl. Instrum. Methods B*, **266**, No. 8: 1647 (2008).
https://doi.org/10.1016/j.nimb.2008.01.043
21. G. Li, J. Wang, J. Du, Y. Ma, T. Liu, and Q. Wang, *J. Magn. Magn. Mater.*, **441**: 448 (2017).
https://doi.org/10.1016/j.jmmm.2017.06.005
22. J.C. Denardin, M. Knobel, L.S. Dorneles, and L.F. Schelp, *Mater. Sci. Engineer. B*, **112**, Nos. 2–3: 120 (2004).
https://doi.org/10.1016/j.mseb.2004.05.016
23. J.L. Maurice, J. Briatico, J. Carrey, F. Petroff, L.F. Schelp, and A. Vaures, *Philos. Mag. A*, **79**, No. 12: 2921 (1999).
https://doi.org/10.1080/01418619908212033
24. W. Wernsdorfer, C. Thirion, N. Demoncy, H. Pascard, and D. Mailly, *J. Magn. Magn. Mater.*, **242–245**, Part 1: 132 (2002).
https://doi.org/10.1016/S0304-8853(01)01153-2
25. O. Kitakami, H. Sato, and Y. Shimada, *Phys. Rev. B*, **56**, No. 21: 13849 (1997).
https://doi.org/10.1103/PhysRevB.56.13849
26. M. Jergel, I. Cheshko, Y. Halahovets, P. Siffalovic, I. Mat'ko, R. Senderak, S. Protsenko, E. Majkova, and S. Luby, *J. Phys. D: Appl. Phys.*, **42**, No. 13: 135406 (2009).
https://doi.org/10.1088/0022-3727/42/13/135406
27. T. Hinotsu, B. Jeyadevan, C.N. Chinnasamy, K. Shinoda, and K. Tohji, *J. Appl. Phys.*, **95**, No. 11: 7477 (2004).
https://doi.org/10.1063/1.1688534
28. V.V. Matveev, D.A. Baranov, G.Yu. Yurkov, N.G. Akatiev, I.P. Dotsenko, and S.P. Gubin, *Chem. Phys. Lett.*, **422**, Nos. 4–6: 402 (2006).
https://doi.org/10.1016/j.cplett.2006.02.099
29. R.H. Kodama and A.S. Edelstein, *J. Appl. Phys.*, **85**, No. 8: 4316 (1999).
https://doi.org/10.1063/1.370354
30. D.I. Saltykov, Yu.O. Shkurdoda, and I.Yu. Protsenko, *J. Nano- Electron. Phys.*, **10**, No. 4: 04031 (2018).
https://doi.org/10.21272/jnep.10(4).04031
31. H. Fujimori, S. Mitani, and S. Ohnuma, *Mater. Sci. Eng. B*, **31**, Nos. 1–2: 219 (1995).
https://doi.org/10.1016/0921-5107(94)08032-1
32. S. Honda and Y. Yamamoto, *J. Appl. Phys.*, **93**, No. 10: 7936 (2003).
https://doi.org/10.1063/1.1555832
33. S. Honda, M. Hirata, M. Ishimaru, *J. Magn. Magn. Mater.*, **290–291**, Part 2: 1053 (2005).

https://doi.org/10.1016/j.jmmm.2004.11.363
34. I.M. Pazukha, Y.O. Shkurdoda, A.M. Chornous and L.V. Dekhtyaruk, *Int. J. Modern Phys. B*, **33**, No. 12: 1950113 (119).
https://doi.org/10.1142/S0217979219501133
35. H. Wang, W.Q. Li, S.P. Wong, W.Y. Cheung, N. Ke, J.B. Xu, X. Lu, and X. Yan, *Mater. Charact.*, **48**, Nos. 2–3: 153 (2002).
https://doi.org/10.1016/S1044-5803(02)00200-0
36. H. Sang, Z.S. Jiang, and Y.W. Du, *J. Magn. Magn. Mater.*, **140–144**, Part 1: 589 (1995).
https://doi.org/10.1016/0304-8853(94)01012-9
37. C. Wang, Z. Guo, Y. Rong, T.Y. Hsu (Xu Zuyao), *Phys. Lett. A*, **329**, No. 3: 236 (2004).
https://doi.org/10.1016/j.physleta.2004.07.004
38. C. Wang, Y. Rong, and T.Y. Hsu (Xu Zuyao), *Mater. Lett.*, **60**, No. 3: 379 (2006).
https://doi.org/10.1016/j.matlet.2005.08.055
39. I.M. Pazukha, D. O. Shuliarenko, O.V. Pylypenko, and L.V. Odnodvorets, *J. Magn. Mater.*, **485**: 89 (2019).
https://doi.org/10.1016/j.jmmm.2019.04.079
40. M. Tamisari, F. Spizzo, M. Sacerdoti, G. Battaglin, and F. Ronconi, *J. Nanopart. Res.*, **13**: 5203 (2011).
https://doi.org/10.1007/s11051-011-0505-x
41. O.V. Stogneĭ, A.V. Sitnikov, Yu.E. Kalinin, S.F. Avdeev, and M.N. Kopytin, *Phys. Solid State*, **49**, No. 1: 164 (2007).
https://doi.org/10.1134/S106378340701026X
42. E.B. Dokukin, R.V. Erhan, A.Kh. Islamov, M.E. Dokukin, N.S. Perov, and E.A. Gan'shina, *Phys. Status Solidi B*, **250**, No. 8: 1656 (2013).
https://doi.org/10.1002/pssb.201248379
43. S. Sankar, A.E. Berkowitz, and D.J. Smith, *Phys. Rev. B*, **62**, No. 21: 14273 (2000).
https://doi.org/10.1103/PhysRevB.62.14273
44. J.C. Slonczewski, *Phys. Rev. B*, **39**, No. 10: 6995 (1989).
https://doi.org/10.1103/PhysRevB.39.6995
45. D.I. Saltykov, Yu.O. Shkurdoda, and I.Yu. Protsenko, *J. Nano- Electron. Phys.*, **10**, No. 3: 03024 (2018).
https://doi.org/10.21272/jnep.10(3).03024
46. A.A. Timopheev, S.M. Ryabchenko, V.M. Kalita, A.F. Lozenko, P.A. Trotsenko, O.V. Stognei, and A.V. Sitnikov, *Phys. Solid State*, **53**, No. 3: 494 (2011).
https://doi.org/10.1134/S1063783411030309
47. A. Vovk, V. Golub, L. Malkinski, A. Kravets, A. Pogoriliy, O. Shipil', *J. Magn. Magn. Mater.*, **272–276**: e1403 (2004).
https://doi.org/10.1016/j.jmmm.2003.12.902
48. A.Ya. Vovk, J.Q. Wang, J.He, W. Zhou, A.M. Pogoriliy, O.V. Shypil', A.F. Kravets, and H.R. Khan, *J. Appl. Phys.*, **91**, No. 12: 10017 (2002).
https://doi.org/10.1063/1.1480113
49. A.Ya. Vovk, V.O. Golub, A.M. Pogoriliy, O.V. Shypil', and A.F. Kravets, *Metallofiz. Noveishie Tekhnol.*, **24**, No. 9: 1277 (2002).
50. A.A. Timofeev, S.M. Ryabchenko, A.F. Lozenko, P.A. Trotsenko, O.V. Stogneĭ, A.V. Sitnikov, and S.F. Avdeev, *Low Temp. Phys.*, **33**, No. 11: 974 (2007).
https://doi.org/10.1063/1.2747075
51. A.E. Varfolomeev and M.V. Sedova, *Phys. Solid State*, **45**, No. 3: 529 (2003).
https://doi.org/10.1134/1.1562242

52. I.M. Melnyk, T.M. Radchenko, and V.A. Tatarenko, *Metallofiz. Noveishie Tekhnol.*, **32**, No. 9: 1191 (2010).
53. T. Sourmail, *Prog. Mater. Sci.*, **50**, No. 7: 816 (2005). https://doi.org/10.1016/j.pmatsci.2005.04.001

Received July 14, 2019;
in final version, November 12, 2019

І.М. Пазуха, В.В. Щоткін, Ю.О. Шкурдода
Сумський державний університет,
вул. Римського-Корсакова, 2, 40007, Суми, Україна

СТРУКТУРА, МАГНЕТНІ ТА МАГНЕТОРЕЗИСТИВНІ ВЛАСТИВОСТІ КОМПОЗИЦІЙНИХ МАТЕРІАЛІВ НА ОСНОВІ ФЕРОМАГНЕТНИХ МЕТАЛІВ І СТОПІВ З РІЗНИМИ ТИПАМИ ДІЕЛЕКТРИЧНОЇ МАТРИЦІ

Представлено літературний огляд експериментальних результатів стосовно структурно-фазового стану, магнеторезистивних і магнетних властивостей тонкоплівкових композитних матеріалів, сформованих на основі ґранул феромагнетного металу Co або стопу Fe_xCo_{1-x}, втілених у діелектричну матрицю (SiO, SiO_2, Al_2O_3) шляхом використання різних метод одержання. Показано, що величина магнетоопору, характер його польових залежностей і магнетні характеристики залежать від концентрації та розподілу за розмірами феромагнетних ґранул. За певних умов у структурах типу феромагнетна ґранула–діелектрична матриця може бути реалізованою перпендикулярна анізотропія, найбільш ймовірні причини виникнення якої проаналізовано.

Ключові слова: композит, феромагнетний матеріал, діелектрична матриця, магнетоопір, магнетні властивості.

И.М. Пазуха, В.В. Щёткин, Ю.А. Шкурдода
Сумский государственный университет,
ул. Римского-Корсакова, 2, 40007 Сумы, Украина

СТРУКТУРА, МАГНИТНЫЕ И МАГНИТОРЕЗИСТИВНЫЕ СВОЙСТВА КОМПОЗИЦИОННЫХ МАТЕРИАЛОВ НА ОСНОВЕ ФЕРРОМАГНИТНЫХ МЕТАЛЛОВ И СПЛАВОВ С РАЗНЫМИ ТИПАМИ ДИЭЛЕКТРИЧЕСКОЙ МАТРИЦЫ

Представлен литературный обзор современных экспериментальных результатов относительно структурно-фазового состояния, магниторезистивных и магнитных свойств тонкоплёночных композитных материалов, сформированных на основе гранул ферромагнитного металла Co или сплава Fe_xCo_{1-x}, внедрённых в диэлектрическую матрицу (SiO, SiO_2, Al_2O_3) при использовании разных методов получения. Показано, что величина магнитосопротивления, характер его полевых зависимостей и магнитные характеристики зависят от концентрации и распределения по размерам ферромагнитных гранул. При определённых условиях в структурах типа ферромагнитная гранула–диэлектрическая матрица может быть реализована перпендикулярная анизотропия, наиболее вероятные причины возникновения которой проанализированы.

Ключевые слова: композит, ферромагнитный материал, диэлектрическая матрица, магнитосопротивление, магнитные свойства.